minerals

MDPI

Article

Patynite, $NaKCa_4[Si_9O_{23}]$, a New Mineral from the Patynskiy Massif, Southern Siberia, Russia

Anatoly V. Kasatkin [1], Fernando Cámara [2], Nikita V. Chukanov [3], Radek Škoda [4], Fabrizio Nestola [5,*], Atali A. Agakhanov [1], Dmitriy I. Belakovskiy [1] and Vladimir S. Lednyov [6]

1 Fersman Mineralogical Museum of Russian Academy of Sciences, Leninsky Prospekt 18-2, 119071 Moscow, Russia; anatoly.kasatkin@gmail.com (A.V.K.); atali99@mail.ru (A.A.A.); dmzvr@mail.ru (D.I.B.)
2 Dipartimento di Scienze della Terra "Ardito Desio", Università degli Studi di Milano, Via Luigi Mangiagalli 34, 20133 Milano, Italy; fernando.camara@unimi.it
3 Institute of Problems of Chemical Physics, Russian Academy of Sciences, Chernogolovka, 142432 Moscow Region, Russia; nikchukanov@yandex.ru
4 Department of Geological Sciences, Faculty of Science, Masaryk University, Kotlářská 2, 61137 Brno, Czech Republic; rskoda@sci.muni.cz
5 Dipartimento di Geoscienze, Università di Padova, Via Gradenigo 6, I-35131 Padova, Italy
6 Khleborobnaya str., 17, 656065 Barnaul, Russia; Lednev68@rambler.ru
* Correspondence: fabrizio.nestola@unipd.it; Tel.: +39-049-827-9160

Received: 13 September 2019; Accepted: 2 October 2019; Published: 5 October 2019

Abstract: The new mineral patynite was discovered at the massif of Patyn Mt. (Patynskiy massif), Tashtagolskiy District, Kemerovo (Kemerovskaya) Oblast', Southern Siberia, Russia. Patynite forms lamellae up to 1 × 0.5 cm and is closely intergrown with charoite, tokkoite, diopside, and graphite. Other associated minerals include monticellite, wollastonite, pectolite, calcite, and orthoclase. Patynite is colorless in individual lamellae to white and white-brownish in aggregates. It has vitreous to silky luster, white streaks, brittle tenacity, and stepped fractures. Its density measured by flotation in Clerici solution is 2.70(2) g/cm^3; density calculated from the empirical formula is 2.793 g/cm^3. The Mohs' hardness is 6. Optically, patynite is biaxial (−) with α = 1.568(2), β = 1.580(2), and γ = 1.582(2) (589 nm). The $2V$ (measured) = 40(10)° and $2V$ (calculated) = 44.1°. The Raman and IR spectra shows the absence in the mineral of H_2O, OH^-, and CO_3^{2-} groups and B–O bonds. The chemical composition is (electron microprobe, wt.%): Na_2O 3.68, K_2O 5.62, CaO 26.82, SiO_2 64.27, total 100.39. The empirical formula based on 23 O *apfu* is $Na_{1.00}K_{1.00}Ca_{4.02}Si_{8.99}O_{23}$. Patynite is triclinic, space group $P\bar{1}$. The unit-cell parameters are: a = 7.27430(10), b = 10.5516(2), c = 13.9851(3) Å, α = 104.203(2)°, β = 104.302(2)°, γ = 92.0280(10)°, V = 1003.07(3) Å^3, Z = 2. The crystal structure was solved by direct methods and refined to R_1 = 0.032. Patynite is an inosilicate with a new type of sextuple branched tubular chain $[(Si_9O_{23})^{10-}]_\infty$ with an internal channel and $[(Si_{18}O_{46})^{20-}]$ as the repeat unit. The strongest lines of the powder X-ray diffraction pattern [d_{obs}, Å (I, %) (hkl)] are: 3.454 (100) (2-1-1), 3.262 (66) (2-1-2), 3.103 (64) (02-4), 2.801 (21), 1.820 (28) (40-2). Type material is deposited in the collections of the Fersman Mineralogical Museum of the Russian Academy of Sciences, Moscow, Russia with the registration number 5369/1.

Keywords: patynite; new mineral; Patynskiy massif; chemistry; new structure type; tubular silicate radical

1. Introduction

Inosilicates represent a very large group of minerals with chain structures. Amongst them, only five mineral species, namely, calcinaksite $KNaCa(Si_4O_{10})\cdot H_2O$ [1], canasite $K_3Na_3Ca_5Si_{12}O_{30}(OH)_4$ [2,3], fluorcanasite $K_3Na_3Ca_5Si_{12}O_{30}F_4\cdot H_2O$ [4], its dimorph frankamenite

$K_3Na_3Ca_5Si_{12}O_{30}(F,OH)_4 \cdot H_2O$ [5,6], and tinaksite $K_2NaCa_2TiSi_7O_{18}(OH)O$ [7–9] are characterized by a very rare feature: the ordering of Na, K, and Ca in their structures.

In the course of the routine SEM/EDS study of the materials sent to the first author for identification by mineral collectors from Southern Siberia, we encountered an unknown mineral containing only Na, K, Ca, Si, and O and having a very unusual Na:K:Ca:Si stoichiometry equal to the 1:1:4:9 ratio. Its further investigation resulted in a discovery of a sixth inosilicate mineral with ordered Na, K, and Ca, however, it is completely different from all five materials mentioned above by the total absence of H_2O, OH, and F, and by a substantially different structure. This new species was named patynite (pronounced pa ty nait; патынитin cyrilic) after the Patynskiy massif in southern Siberia where it has been found.

The mineral and its name have been approved by the IMA Commission on New Minerals, Nomenclature and Classification (IMA no. 2019-018). Type material is deposited in the collections of the Fersman Mineralogical Museum of the Russian Academy of Sciences, Moscow, Russia, with the registration number 5369/1.

2. Occurrence, Geological Settings, and Mineral Association

Samples containing the new mineral were found in August 2018 during a field trip made by a group of amateur mineralogists from Altay Krai lead by one of the authors (V.S.L.) to Gornaya Shoriya, a mountainous-taiga region located in the South of Kemerovo (Kemerovskaya) Oblast', Southern Siberia, Russia. More precisely, the new mineral was collected in the massif of Patyn Mt. (aka Patynskiy massif) located in the central part of Gornaya Shoriya, in the Tashtagolskiy District of Kemerovo Oblast' (Figure 1). Geographical coordinates of the locality are 53°3′32″ N and 88°44′29″ E.

Figure 1. Patynskiy massif: general view from Mt. Patyn. August, 2018. Photo: Vladimir S. Lednyov.

Geologically, Patynskiy massif belongs to an Early Devonian gabbro-syenite formation. It occupies an approximate area of 50 km^2 and has an isometric outline. Its contacts fall from the periphery to the central part showing a funnel form of the massif. Patynskiy massif was formed in near-surface conditions and, most probably, represents a subvolcano. It is composed mainly of basic rocks including different types of gabbro (olivine and titanomagnetite ones with coarse grained pegmatoid, vesicular, and porphyritic textures), as well as troctolites, norites, pyroxenites, anorthosites, etc. Other types of rocks are represented by rare dikes of microgranites, selvsbergites, grorudites, veins of monticellite–melilite–nepheline rocks, acid and alkaline pegmatites, and alkaline syenites. While basic

rocks are strongly dominant throughout the massif and show a concentric-zonal structure, other ones are spread out locally in central and south-western parts of the massif. All these rocks are studied in detail and described in the geologic literature [10–13].

The north-eastern part of Patynskiy massif has been rarely studied; it was considered by geologists as unpromising for industrial mineralization. In this area, the collecting group discovered an outcrop of diopside-wollastonite skarns, 15 m in width, confined to the contact of pyroxenite with marmorized limestone. The samples containing patynite were collected approximately 200 m from the outcrop, in the alluvium of the small river Pravyi (Right) Sunzas (a left tributary of the Bazas river), 2 km below its head (Figure 2).

Figure 2. Alluvium of the Pravyi Sunzas river where patynite was collected. August 2018. Photo: Vladimir S. Lednyov.

The new mineral was discovered in a single large boulder measuring 70 × 50 × 40 cm in size and weighing 50 kg (Figure 3). Its main part consists of white to light blue fine-grained diopside closely intergrown with snow-white monticellite and pale-blue wollastonite-2*M*. Patynite occurs in the middle part of the boulder as lamellar aggregates with a characteristic stepped fracture, intimately intergrown with charoite, tokkoite, white and green diopside, and graphite. Other minerals found in the boulder were pectolite, calcite, and orthoclase. This assemblage and the place of patynite discovery indicate that this mineral has a metasomatic origin and most likely comes from the above-mentioned skarns.

The mineral association of patynite with charoite and tokkoite is noteworthy. The two latter minerals were discovered in charoitites of the Murun alkaline massif in Eastern Siberia [8,9,14–17], and until the present time, were considered as endemics. Our find is, therefore, the second in the world for both of these minerals.

Similar to the charoite from Murun, this one from the Patynskiy massif forms long-fibrous aggregates with vitreous to silky luster and has good cleavage in three directions. The main difference between the charoite varieties from the two localities is the color. Charoite from its type locality is famous for purple to violet coloration caused by traces of Mn^{3+}, whereas charoite from the Patynskiy massif is whitish-grey to brown. Its chemical composition is as follows (wt.%, average of five analyses, H_2O calculated from the deficiency of the analysis total): Na_2O 1.87; K_2O 9.11; CaO 24.63; MnO 0.03; BaO 0.90; SiO_2 59.76; H_2O 3.70; total 100.00. It corresponds to the following empirical formula (calculated on the basis of 70 Si *apfu* with the OH/H_2O ratio determined from the charge-balance condition): $(K_{13.61}Ba_{0.41}Mn_{0.02})_{\Sigma 14.04}(Ca_{30.91}Na_{4.25})_{\Sigma 35.61}Si_{70}[O_{171.77}(OH)_{13}]_{\Sigma 184.77}(OH)_4 \cdot 5.95H_2O$.

This formula is, in general, consistent with the crystal-chemical formula of charoite from Murun, $(K_{13.88}Sr_{1.00}Ba_{0.32}Mn_{0.36})_{\Sigma 15.56}(Ca_{25.64}Na_{6.36})_{\Sigma 32}[Si_{70}(O_{170.88}(OH)_{9.12}]_{\Sigma 180}(OH,F)_4 \cdot 3.18H_2O$ [15], differing from the latter by the total absence of admixed Sr and F and a substantially higher Ca content. The monoclinic unit-cell dimensions calculated from the powder X-ray diffraction pattern of charoite from the Patynskiy massif are: a = 31.859(3), b = 19.642(2), c = 7.095(2) Å, β = 90.02(1)°, V = 4440.1(8) Å^3. These are very close to the refined parameters of charoite from the type locality: a = 31.96(6), b = 19.64(4), c = 7.09(1) Å, β = 90.0(1)°, V = 4450(24) Å^3 [16].

Figure 3. Large, diopside–monticellite–wollastonite boulder with the middle part consisting of patynite, charoite, tokkoite, diopside, and graphite. August 2018. Photo: Vladimir S. Lednyov.

Tokkoite from the Patynskiy massif forms platy aggregates overgrowing charoite. They are colorless, with vitreous luster and two directions of cleavage: perfect on {010} and good on {110}. The chemical composition is (wt.%, average of five analyses, H_2O calculated by stoichiometry): K_2O 12.53; CaO 29.43; MnO 0.04; SiO_2 55.19; H_2O 1.33; F 2.20; –O=F –0.93; total 99.61. Amazingly, it corresponds to an almost end-member formula (calculated on the basis of 20 O + F atoms *pfu*): $K_{2.00}Ca_{4.00}Si_{7.00}O_{18}(OH)[F_{0.88}(OH)_{0.12}]$. For comparison, different chemical analyses of tokkoite from its type locality always show the presence of various admixed cations, such as Na, Mg, Mn^{2+}, Fe^{2+}, and Fe^{3+} substituting for Ca in structural sites [8,9,17]. The triclinic unit-cell dimensions calculated from the powder X-ray diffraction pattern of tokkoite from Patynskiy massif are: a = 10.404(2), b = 12.528(2), c = 7.087(1) Å, α = 89.80(1)°, β = 99.60(1)°, γ = 92.72(1)°, V = 909.9(2) Å^3. They correspond well to the average crystallographic data given in the most recent paper on the crystal structure of tokkoite from Murun: $a \approx 10.423$, $b \approx 12.477$, $c \approx 7.112$ Å, α ≈ 89.92°, β ≈ 99.68°, γ ≈ 92.97°, $V \approx 910.5$ Å^3 [9].

3. Methods

The Raman spectrum of patynite was obtained from a polished section by means of a Horiba Labram HR Evolution spectrometer (Jobin Yvon, Palaiseau, France. This dispersive, edge-filter-based system is equipped with an Olympus BX 41 optical microscope (Olympus Company, Shinjuku, Japan), a diffraction grating with 600 grooves per millimeter, and a Peltier-cooled, Si-based charge-coupled device (CCD) detector. After careful tests with different lasers (473, 532, and 633 nm), the 633 nm He–Ne laser with the beam power of 10 mW at the sample surface was selected for spectra acquisition to minimize analytical artefacts. Raman signal was collected in the range of 100–4000 cm^{-1} with a 100x

objective (NA 0.9) and the system operated in the confocal mode, beam diameter was ~1 μm, and the lateral resolution ~2 μm. No visual damage of the analyzed surface was observed at these conditions after the excitation. Wavenumber calibration was done using the Rayleigh line and low-pressure Ne-discharge lamp emissions. The wavenumber accuracy was ~0.5 cm^{-1}, and the spectral resolution was ~2 cm^{-1}. Band fitting was done after appropriate background correction, assuming combined Lorentzian–Gaussian band shapes using the Voight function (*PeakFit*; Version number 4.12, originally developed by Jandel Scientific, Erkraht, Germany, now distributed by Systat software Inc., San Jose, CA, USA).

In order to obtain the IR absorption spectrum of patynite, hand-picked fragments were ground in an agate mortar, mixed with anhydrous KBr, pelletized, and analyzed using an ALPHA FTIR spectrometer (Bruker Optics, Ettlingen, Germany) in the range of wavenumbers from 360 to 3800 cm^{-1}, with a spectral resolution of 4 cm^{-1}. The IR spectrum of a pure KBr disk was used as a reference.

Chemical analyses (11 points) were carried out with a Cameca SX-100 electron microprobe (Cameca company, part of Ametek group, Gennevilliers Cedex, France) (WDS mode, 15 kV, 10 nA, 8 μm beam diameter). The following standards were used: albite for Na, orthoclase for K, andradite for Ca, and sanidine for Si. No other elements were found above the detection limit. Raw intensities were processed by the X-PHI matrix correction algorithm.

The single-crystal X-ray diffraction experiment was carried out on a grain of patynite with the size 0.10 × 0.06 × 0.02 mm^3. It was extracted from the polished section, analyzed using electron microprobe, then mounted on a glass fiber and examined with a Supernova Rigaku-Oxford Diffraction diffractometer (Rigaku-Oxford Diffraction, Neu Isenbrug, Germany) equipped with a Pilatus 200 K Dectris detector (Dectris, Baden-Daettwil, Switzerland) and a X-ray micro-source (MoKα radiation) with spot of 0.12 mm. The detector-to-sample distance was 68 mm. A full sphere of three-dimensional data was collected. Data reduction was performed using CrysAlisPro (Rigaku-Oxford Diffraction, Neu Isenbrug, Germany). The data were corrected for Lorentz factor and polarization effect, and the absorption correction was performed by running the interframe scaling implemented in CrysAlisPro (ver. 1.171.40.55a, Neu Isenbrug, Germany).

Powder X-ray diffraction data were collected using the same X-ray instrument, which can act as a micro-powder diffractometer. A standard phi scan mode (0–360° rotation) as implemented in the powder power tool of CrysAlis Pro ver. 1.171.40.55a was used for the powder data collection.

4. Results

4.1. General Appearance, Physical, Chemical, and Optical Properties

Patynite forms lamellar aggregates up to 1 × 0.5 cm and is closely intergrown with charoite, tokkoite, diopside, and graphite (Figures 4–6). The new mineral is transparent, colorless in individual lamellae to white and white-brownish in aggregates. It has vitreous to silky luster and white streaks. The mineral is brittle, with a stepped fracture. Patynite shows two directions of perfect cleavage parallel to the individuals' elongation and one imperfect cleavage with 96° to the individuals' elongation. Parting was not observed. The new mineral itself is not fluorescent, however, macro specimens containing patynite show bright green fluorescence under SW UV radiation, presumably due to absorbed, very thin films of unidentified, amorphous uranyl-bearing Al-Si minerals filling the microcracks at the contacts of patynite with the associated minerals. Its density measured by flotation in Clerici solution is 2.70(2) g/cm^3; density calculated from the empirical formula is 2.793 g/cm^3. The Mohs' hardness based on scratching tests is 6. The mineral does not react with cold hydrochloric and nitric acids.

Figure 4. White and brownish-white patynite closely intergrown with charoite, tokkoite, diopside, and graphite.

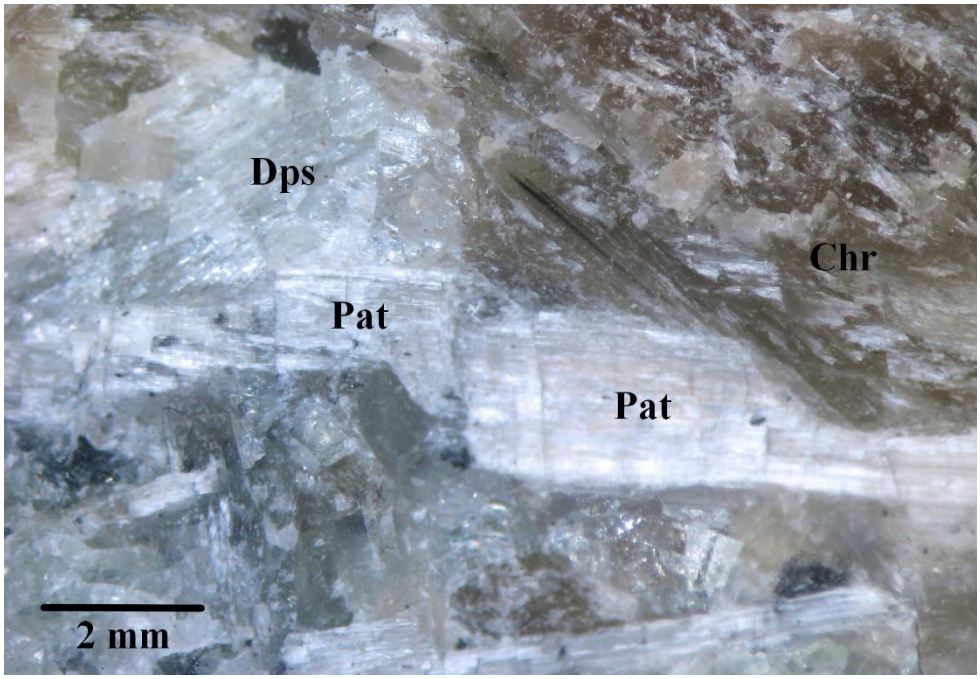

Figure 5. Close-up of the sample pictured at Figure 4. White lamellar aggregates of patynite (Pat) with brown fibrous charoite (Chr), and colorless diopside (Dps). Black grains are graphite.

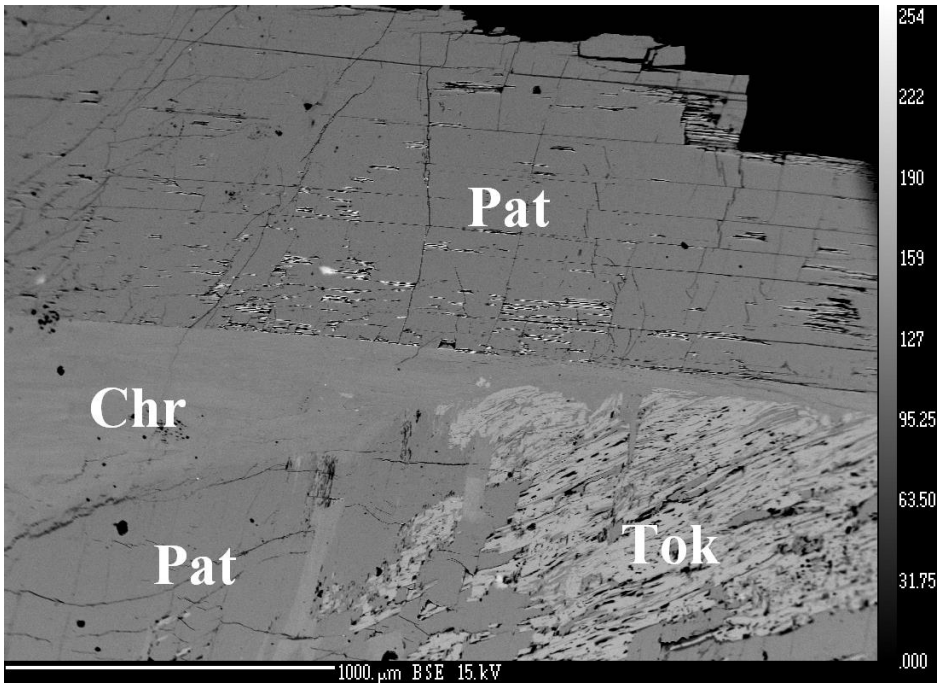

Figure 6. Patynite (Pat) intergrown with charoite (Chr) and tokkoite (Tok). Polished section. SEM image (BSE mode).

In transmitted plain polarized light, patynite is colorless and non-pleochroic. It is optically biaxial (−) with α = 1.568(2), β = 1.580(2), γ = 1.582(2) (589 nm). The $2V$ estimated based on the curve of the conoscopical figure for the section perpendicular to the optical axis is 40(10)°, $2V$ (calculated) = 44.1°. Dispersion of optical axes is weak, $r < v$. Optical Y axis is nearly parallel to the individuals' elongation.

The Gladstone–Dale compatibility index ($1 - K_p/K_c$) is 0.003, using the empirical formula and the unit-cell parameters determined from single-crystal X-ray data, which is rated as "superior" [18].

4.2. Raman Spectroscopy

The Raman spectrum of patynite (Figure 7) shows the absence of absorption bands of H_2O molecules, OH groups, and CO_3^{2-} anions. The bands in the range of 1000–1200 cm^{-1} correspond to stretching vibrations of the Si–O–Si fragments, and the bands in the range of 900–1000 cm^{-1} are due to stretching vibrations of apical Si–O bonds. The bands in the 720–820 cm^{-1} range can be assigned to complex vibrations of tetrahedral rings ("ring bands" [19]), while those in the 600–700 cm^{-1} range can be assigned to O–Si–O bending vibrations. The bands below 600 cm^{-1} correspond to lattice modes involving Si–O–Si bending and Ca–O-stretching vibrations, as well as (below 200 cm^{-1}) Na–O- and K–O-stretching vibrations.

Assignment of the weak band at 1326 cm^{-1} is ambiguous. This band could correspond to trace amounts of B–O bonds, but IR spectroscopic data exclude this possibility. Therefore, we assign this band to a combination mode.

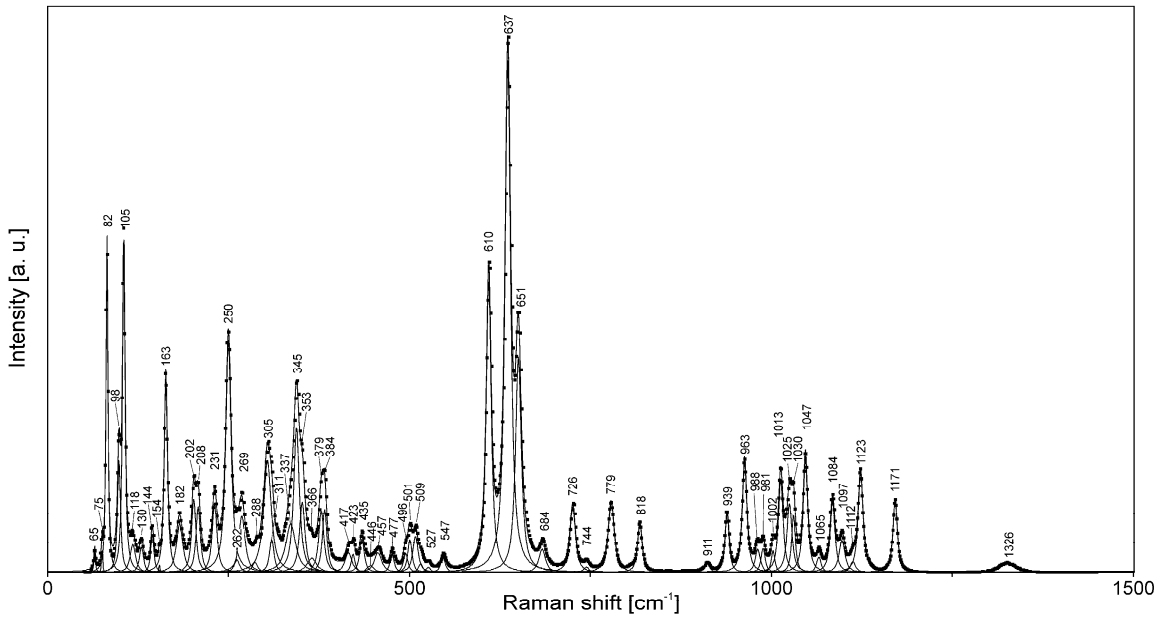

Figure 7. Raman spectrum of patynite excited by 633 nm laser in the 50–1500 cm^{-1} region. The measured spectrum is shown by dots. The curve matching to dots is a result of spectral fit as a sum of individual Voigt peaks shown below the curve.

4.3. Infrared Spectroscopy

The IR spectrum of patynite (Figure 8) is unique and can be used as a reliable diagnostic tool. The assignment of IR absorption bands (ranges) are as follows:

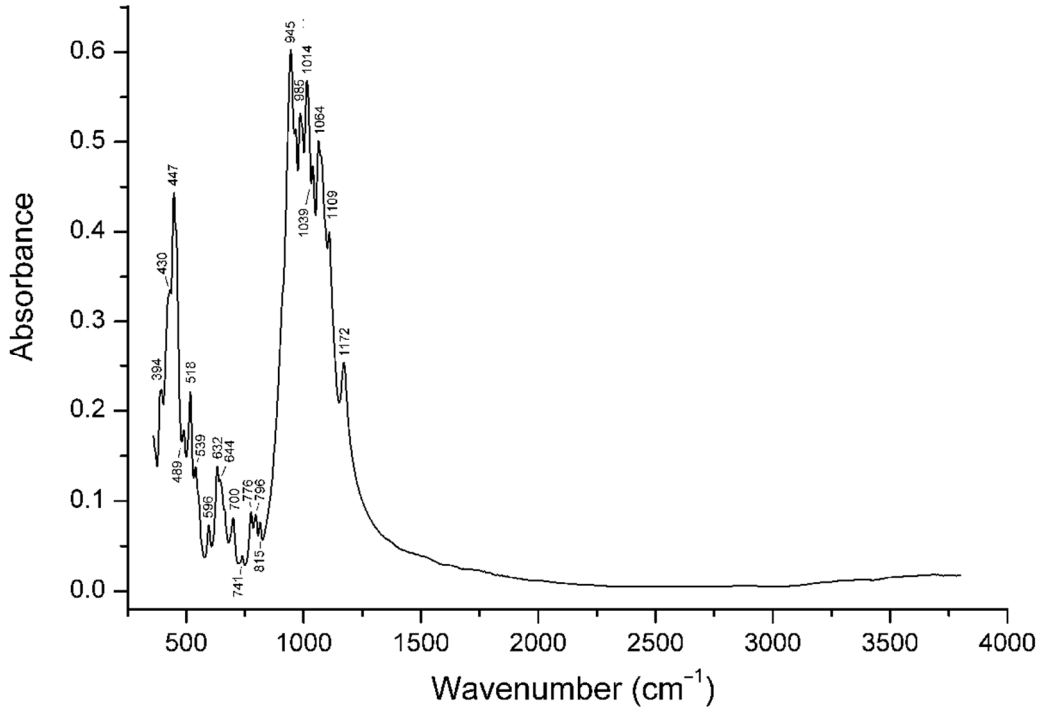

Figure 8. Infrared absorption spectrum of patynite.

1014–1172 cm^{-1}: stretching vibrations of the Si–O–Si fragments;
945 and 985 cm^{-1}: stretching vibrations of apical Si–O bonds;
741–815 cm^{-1}: complex vibrations of tetrahedral rings (“ring bands”);

596–700 cm^{-1}: O–Si–O bending vibrations;

Bands below 540 cm^{-1}: lattice modes involving Si–O–Si bending and Ca–O-stretching vibrations.

No bands of H_2O, OH^-, or CO_3^{2-} groups or B–O bonds were observed in the IR spectrum of patynite.

There is a simple correlation between the weighted average frequency $\langle\nu_{Si-O}\rangle$ of the (Si,Al)–O-stretching vibrations (in the range from 820 to 1200 cm^{-1}) and the mean number of vertices that a $(Si,Al)O_4$ tetrahedron shares with other tetrahedra [20]. In particular, for aluminosilicates with the stoichiometry of the tetrahedral part $Si_xAl_yO_z$, the correlation is as follows:

$$\langle\nu_{Si-O}\rangle\ (cm^{-1}) = (337.8t + 1827)(0.6428t + 1)^{-1}, \text{ where } t = z(x + 0.5y)^{-1}.$$

Consequently, for silicates that do not contain aluminum in the tetrahedral part, the following correlation is valid: $t = (1827 - \langle\nu_{Si-O}\rangle)(0.6428\langle\nu_{Si-O}\rangle - 337.8)^{-1}$, where t is the atomic O:Si ratio in the tetrahedral part of the crystal structure. For patynite, $\langle\nu_{Si-O}\rangle \approx 1020\ cm^{-1}$, which corresponds to $t = 2.54$. This value is close to the t value of 2.556 calculated from the idealized formula.

4.4. Chemical Composition

Chemical data for patynite are given in Table 1. Contents of other elements with atomic numbers >8 are below detection limits.

Table 1. Chemical data for patynite.

Constituent	wt.%	Range	Standard Deviation
Na_2O	3.68	3.25–4.04	0.25
K_2O	5.62	5.48–5.98	0.17
CaO	26.82	26.63–27.12	0.15
SiO_2	64.27	64.03–64.49	0.17
Total	100.39		

The empirical formula (calculated on the basis of 23 O *apfu*) is $Na_{1.00}K_{1.00}Ca_{4.02}Si_{8.99}O_{23}$.

The ideal formula is $NaKCa_4[Si_9O_{23}]$, which requires Na_2O 3.68, K_2O 5.59, CaO 26.60, and SiO_2 64.13, total 100 wt.%.

4.5. X-ray Diffraction Data

The crystal structure of patynite was solved by direct methods based on single-crystal X-ray diffraction data and refined using the SHELX-97 software within the WINGX package [21,22] to $R_1 = 0.032$ for 10,758 unique reflections with $I > 2\sigma(I)$. All atoms were refined anisotropically. Patynite is triclinic, space group $P\bar{1}$. The refined unit-cell parameters are: $a = 7.27430(10)$, $b = 10.5516(2)$, $c = 13.9851(3)$ Å, $\alpha = 104.203(2)°$, $\beta = 104.302(2)°$, $\gamma = 92.0280(10)°$, $V = 1003.07(3)$ $Å^3$; $Z = 2$.

The crystal data and the experimental details are presented in Table 2, atom coordinates, thermal displacement parameters in Tables 3 and 4, and selected interatomic distances in Table 5. In order to show the lack of evidence of oxygen–hydrogen bonds, the Bond valence calculations are given in Table 6.

Powder X-ray diffraction data are presented in Table 7. The unit-cell parameters refined from the powder data using UNITCELL software by Holland and Redfern [23] are as follows: $a = 7.2708(6)$, $b = 10.5244(10)$, $c = 13.9527(16)$ Å, $\alpha = 104.136(11)°$, $\beta = 104.315(8)°$, $\gamma = 91.840(11)°$, $V = 998.32(13)$ $Å^3$; $Z = 2$.

Table 2. Crystal data, data collection information, and structure refinement details for patynite.

Formula: $Ca_4KNaSi_9O_{23}$	$R[F^2 > 2\sigma(F^2)] = 0.032$
Symmetry: triclinic	$wR(F^2) = 0.088$
Space group: $P\bar{1}$	$S = 1.38$
$Mr = 843.22$	12,417 reflections, 349 parameters
$a = 7.27420(10)$ Å	$F(000) = 840$
$b = 10.5516(2)$ Å	Mo $K\alpha$ radiation, $\lambda = 0.71073$ Å
$c = 13.9851(3)$ Å	$\mu = 1.97$ mm^{-1}
A = 104.20°	$T = 293$ K
β = 104.302(2)°	Rint = 0.074
γ = 92.0280(10)°	$\theta_{max} = 40.3°$, $\theta_{min} = 1.6°$
$V = 1003.07(3)$ Å^3	$h = -13 \rightarrow 13$
$Z = 2$	$k = -19 \rightarrow 19$
$D_x = 2.792$ g cm^{-3}	$l = -25 \rightarrow 25$
Radiation source: fine-focus sealed tube	Secondary atom site location: difference Fourier map
Graphite monochromator	$[0.00000 + 1.00000\exp(1.30(\sin\theta/\lambda)^2)]/[\sigma^2(F_o^2) + 0.0000 + 0.0448 \times P + (0.0377P)^2 + 0.0000\sin\theta/\lambda]$ where $P = 0.33333F_o^2 + 0.66667F_c^2$
64,993 measured reflections	$(\Delta/\sigma)_{max} = 0.002$
12,417 independent reflections	$\Delta\rho_{max} = 0.89$ e Å^{-3}
10,758 reflections with $I > 2\sigma(I)$	$\Delta\rho_{min} = -0.84$ e Å^{-3}

Table 3. Fractional atomic coordinates and equivalent isotropic displacement parameters (Å^2) for patynite.

Site	x	y	z	U_{eq}
Ca1	0.82421 (3)	0.51657 (2)	0.381141 (17)	0.00783 (5)
Ca2	1.31382 (3)	0.90730 (2)	0.382301 (17)	0.00894 (6)
Ca3	0.81839 (3)	0.89891 (2)	0.366450 (17)	0.00896 (6)
Ca4	1.32069 (3)	0.50733 (2)	0.383805 (17)	0.00822 (5)
Na1	0.49261 (10)	0.16604 (6)	0.24880 (5)	0.01881 (18)
K1	0.95296 (5)	0.31141 (3)	0.06920 (2)	0.01780 (8)
Si1	0.81655 (4)	0.23437 (3)	0.46046 (2)	0.00626 (5)
Si2	0.61746 (4)	0.76796 (3)	0.53758 (2)	0.00604 (5)
Si3	1.01727 (4)	0.23158 (3)	0.29416 (2)	0.00660 (5)
Si4	0.65171 (4)	0.80298 (3)	0.03303 (2)	0.00661 (5)
Si5	1.00983 (4)	0.97746 (3)	0.16364 (2)	0.00648 (5)
Si6	1.37874 (4)	0.88172 (3)	0.15444 (2)	0.00695 (5)
Si7	0.78112 (4)	0.60955 (3)	0.16865 (2)	0.00716 (5)
Si8	1.21164 (4)	0.62856 (3)	0.18476 (2)	0.00689 (5)
Si9	0.47777 (4)	0.40913 (3)	0.16444 (2)	0.00644 (5)
O1	0.88140 (12)	0.38775 (8)	0.51075 (7)	0.00927 (13)
O2	1.21329 (12)	0.97974 (9)	0.13360 (7)	0.01035 (13)
O3	1.50826 (12)	0.93270 (9)	0.26821 (7)	0.01100 (14)
O4	0.58346 (12)	0.21518 (10)	0.43054 (7)	0.01196 (14)
O5	0.89613 (12)	0.12808 (9)	0.51932 (7)	0.01073 (13)

Table 3. *Cont.*

Site	x	y	z	U_{eq}
Ca1	0.82421 (3)	0.51657 (2)	0.381141 (17)	0.00783 (5)
Ca2	1.31382 (3)	0.90730 (2)	0.382301 (17)	0.00894 (6)
Ca3	0.81839 (3)	0.89891 (2)	0.366450 (17)	0.00896 (6)
Ca4	1.32069 (3)	0.50733 (2)	0.383805 (17)	0.00822 (5)
Na1	0.49261 (10)	0.16604 (6)	0.24880 (5)	0.01881 (18)
K1	0.95296 (5)	0.31141 (3)	0.06920 (2)	0.01780 (8)
Si1	0.81655 (4)	0.23437 (3)	0.46046 (2)	0.00626 (5)
Si2	0.61746 (4)	0.76796 (3)	0.53758 (2)	0.00604 (5)
Si3	1.01727 (4)	0.23158 (3)	0.29416 (2)	0.00660 (5)
Si4	0.65171 (4)	0.80298 (3)	0.03303 (2)	0.00661 (5)
Si5	1.00983 (4)	0.97746 (3)	0.16364 (2)	0.00648 (5)
Si6	1.37874 (4)	0.88172 (3)	0.15444 (2)	0.00695 (5)
Si7	0.78112 (4)	0.60955 (3)	0.16865 (2)	0.00716 (5)
Si8	1.21164 (4)	0.62856 (3)	0.18476 (2)	0.00689 (5)
Si9	0.47777 (4)	0.40913 (3)	0.16444 (2)	0.00644 (5)
O1	0.88140 (12)	0.38775 (8)	0.51075 (7)	0.00927 (13)
O2	1.21329 (12)	0.97974 (9)	0.13360 (7)	0.01035 (13)
O3	1.50826 (12)	0.93270 (9)	0.26821 (7)	0.01100 (14)
O4	0.58346 (12)	0.21518 (10)	0.43054 (7)	0.01196 (14)
O5	0.89613 (12)	0.12808 (9)	0.51932 (7)	0.01073 (13)
O6	0.79457 (14)	0.67329 (9)	0.28513 (7)	0.01174 (14)
O7	1.02215 (13)	0.92523 (9)	0.26198 (7)	0.01069 (13)
O8	1.02637 (13)	0.38183 (9)	0.29368 (7)	0.01073 (13)
O9	0.52356 (12)	0.40238 (9)	0.28020 (6)	0.00956 (13)
O10	0.66264 (12)	0.46186 (9)	0.13305 (7)	0.01013 (13)
O11	1.26701 (13)	0.73514 (9)	0.12639 (7)	0.01143 (14)
O12	0.62744 (12)	0.61611 (8)	0.48453 (7)	0.00912 (13)
O13	0.40927 (13)	0.25908 (8)	0.09035 (6)	0.00955 (13)
O14	0.63569 (12)	0.88002 (9)	0.48068 (7)	0.00999 (13)
O15	0.77274 (12)	0.80587 (9)	0.65113 (7)	0.01171 (14)
O16	1.28126 (13)	0.67805 (9)	0.30517 (7)	0.01079 (13)
O17	0.48846 (13)	0.88853 (9)	0.06690 (7)	0.01199 (14)
O18	0.85399 (13)	0.19139 (10)	0.34567 (7)	0.01196 (14)
O19	0.66731 (13)	0.68766 (10)	0.08966 (8)	0.01312 (15)
O20	1.29865 (13)	0.49326 (9)	0.13704 (7)	0.01187 (14)
O21	0.85363 (12)	0.88962 (9)	0.06076 (7)	0.01119 (14)
O22	0.98268 (12)	0.58570 (9)	0.13860 (7)	0.01107 (14)
O23	0.95847 (12)	0.13084 (8)	0.17922 (6)	0.00831 (12)

Table 4. Anisotropic displacement parameters (in Å^2) for patynite.

Site	U^{11}	U^{22}	U^{33}	U^{12}	U^{13}	U^{23}
O6	0.0162 (4)	0.0109 (3)	0.0081 (3)	0.0008 (3)	0.0032 (3)	0.0023 (3)
O7	0.0110 (3)	0.0134 (3)	0.0089 (3)	0.0016 (3)	0.0019 (3)	0.0059 (3)
O8	0.0114 (3)	0.0083 (3)	0.0111 (3)	0.0005 (2)	0.0011 (3)	0.0020 (3)
O9	0.0101 (3)	0.0116 (3)	0.0059 (3)	0.0002 (2)	0.0004 (2)	0.0022 (2)
O10	0.0089 (3)	0.0093 (3)	0.0125 (3)	−0.0006 (2)	0.0036 (3)	0.0029 (3)
O11	0.0137 (3)	0.0103 (3)	0.0102 (3)	−0.0021 (3)	0.0017 (3)	0.0043 (3)
O12	0.0103 (3)	0.0072 (3)	0.0085 (3)	0.0012 (2)	0.0005 (2)	0.0014 (2)
O13	0.0130 (3)	0.0081 (3)	0.0059 (3)	−0.0007 (2)	0.0009 (2)	0.0005 (2)
O14	0.0120 (3)	0.0100 (3)	0.0094 (3)	0.0012 (2)	0.0032 (3)	0.0048 (3)
O15	0.0081 (3)	0.0157 (4)	0.0076 (3)	0.0027 (3)	−0.0025 (2)	0.0006 (3)
O16	0.0133 (3)	0.0108 (3)	0.0074 (3)	0.0008 (3)	0.0004 (3)	0.0032 (3)
O17	0.0141 (3)	0.0133 (4)	0.0139 (4)	0.0062 (3)	0.0088 (3)	0.0074 (3)
O18	0.0110 (3)	0.0165 (4)	0.0080 (3)	−0.0011 (3)	0.0049 (3)	0.0005 (3)
O19	0.0124 (3)	0.0138 (4)	0.0148 (4)	0.0026 (3)	0.0005 (3)	0.0097 (3)
O20	0.0102 (3)	0.0109 (3)	0.0129 (3)	0.0048 (3)	0.0010 (3)	0.0016 (3)
O21	0.0096 (3)	0.0128 (3)	0.0087 (3)	−0.0025 (3)	0.0002 (3)	0.0011 (3)
O22	0.0066 (3)	0.0136 (4)	0.0119 (3)	0.0002 (2)	0.0017 (3)	0.0021 (3)
O23	0.0104 (3)	0.0078 (3)	0.0055 (3)	0.0027 (2)	0.0003 (2)	0.0010 (2)

Table 5. Selected interatomic distances (Å) in the structure of patynite (for more geometrical parameters see the CIF file in Supplementary Materials).

Ca1–O1^{i}	2.3214 (9)	Ca2–O5^{i}	2.3696 (9)
Ca1–O6	2.3571 (9)	Ca2–O16	2.3715 (9)
Ca1–O12	2.3720 (9)	Ca2–O7	2.4062 (9)
Ca1–O9	2.3834 (9)	Ca2–O3	2.4324 (9)
Ca1–O8	2.4214 (9)	Ca2–O14^{ii}	2.4715 (9)
Ca1–O1	2.4865 (9)	Ca2–O14^{iii}	2.5153 (9)
<Ca1–O>	2.390	<Ca2–O>	2.428
Ca3–O6	2.3528 (10)	Ca4–O16	2.3215 (9)
Ca3–O14	2.3546 (9)	Ca4–O8	2.3607 (9)
Ca3–O5^{i}	2.3605 (9)	Ca4–O12^{ii}	2.3985 (9)
Ca3–O7	2.3767 (9)	Ca4–O9^{ii}	2.4265 (9)
Ca3–O3^{iv}	2.4228 (9)	Ca4–O1^{i}	2.4385 (9)
Ca3–O5^{v}	2.7398 (10)	Ca4–O12^{i}	2.4694 (9)
<Ca3–O>	2.435	<Ca4–O>	2.403

Table 5. *Cont.*

Na1–O4	2.3800 (12)	K1–O11^{viii}	2.7214 (10)
Na1–O9	2.4159 (11)	K1–O23	2.7226 (9)
Na1–O3^{vi}	2.5457 (11)	K1–O22	2.7998 (10)
Na1–O13	2.5860 (11)	K1–O10	2.8724 (9)
Na1–O18	2.6134 (12)	K1–O20	2.9141 (10)
Na1–O15^{vii}	2.6351 (12)	K1–O8	2.9483 (10)
Na1–O2^{vi}	2.6709 (11)	K1–O21^{viii}	3.0601 (10)
<Na1–O>	2.550	K1–O13^{ii}	3.3369 (10)
		<K1–O>	2.922
Si1–O5	1.5919 (9)	Si2–O14	1.5974 (9)
Si1–O1	1.6000 (9)	Si2–O12	1.6044 (9)
Si1–O4	1.6355 (9)	Si2–O4^{vii}	1.6334 (9)
Si1–O18	1.6505 (9)	Si2–O15	1.6515 (9)
<Si1–O>	1.619	<Si2–O>	1.622
Si3–O8	1.5861 (9)	Si4–O19	1.5996 (9)
Si3–O18	1.6268 (9)	Si4–O21	1.6103 (9)
Si3–O23	1.6390 (9)	Si4–O17	1.6104 (9)
Si3–O15^{i}	1.6397 (9)	Si4–O13^{x}	1.6278 (9)
<Si3–O>	1.623	<Si4–O>	1.612
Si5–O7	1.5868 (9)	Si6–O3	1.5849 (9)
Si5–O2	1.6361 (9)	Si6–O11	1.6317 (9)
Si5–O21	1.6382 (9)	Si6–O17^{ii}	1.6317 (9)
Si5–O23^{v}	1.6481 (9)	Si6–O2	1.6327 (9)
<Si5–O>	1.627	<Si6–O>	1.620
Si7–O6	1.5794 (10)	Si8–O16	1.5791 (9)
Si7–O19	1.6212 (9)	Si8–O22	1.6332 (9)
Si7–O22	1.6335 (9)	Si8–O11	1.6353 (9)
Si7–O10	1.6527 (9)	Si8–O20	1.6399 (9)
<Si7–O>	1.622	<Si8–O>	1.622
Si9–O9	1.5902 (9)		
Si9–O20^{iv}	1.6232 (9)		
Si9–O10	1.6339 (9)		
Si9–O13	1.6470 (9)		
<Si9–O>	1.624		

Symmetry codes: (i) $-x + 2, -y + 1, -z + 1$; (ii) $x + 1, y, z$; (iii) $-x + 2, -y + 2, -z + 1$; (iv) $x - 1, y, z$; (v) $x, y + 1, z$; (vi) $x - 1, y - 1, z$; (vii) $-x + 1, -y + 1, -z + 1$; (viii) $-x + 2, -y + 1, -z$; (ix) $x, y - 1, z$; (x) $-x + 1, -y + 1, -z$; (xi) $x + 1, y + 1, z$. Document origin: *publCIF* [24].

Table 6. Bond-valence calculations for patynite.

	K	Ca1	Ca2	Ca3	Ca4	Na1	Si1	Si2	Si3	Si4	Si5	Si6	Si7	Si8	Si9	Σ
O1	-	0.363 0.242	-	-	0.273	-	1.064	-	-	-	-	-	-	-	-	1.942
O2	-	-	-	-	-	0.098	-	-	-	-	0.969	0.934	-	-	-	2.001
O3	-	-	0.277	0.283	-	0.132	-	-	-	-	-	1.086	-	-	-	1.778
O4	-	-	-	-	-	0.196	0.971	0.976	-	-	-	-	-	-	-	2.143
O5	-		0.323	0.330 0.131	-	-	1.086	-	-	-	-	-	-	-	-	1.739
O6	-	0.331	-	0.336	-	-	-	-	-	-	-	-	1.071	-	-	1.740
O7	-	-	0.295	0.317	-	-	-	-	-	-	1.100	-	-	-	-	1.713
O8	0.104	0.284	-	-	0.330	-	-	-	1.102	-	-	-	-	-	-	1.820
O9	-	0.312	-	-	0.281	0.180	-	-	-	-	-	-	-	-	1.065	1.837
O10	0.126	-	-	-	-	-	-	-	-	-	-	-	0.932	-	1.036	2.093
O11	0.184	-	-	-	-	-	-	-	-	-	-	1.064	-	0.962	-	2.210
O12	-	0.321	-	-	0.301 0.253	-	-	1.052	-	-	-	-	-	-	-	1.926
O13	0.039	-	-	-	-	0.120	-	-	-	0.990	-	-	-	-	0.990	2.140
O14	-	-	0.252 0.226	0.335	-	-	-	1.071	-	-	-	-	-	-	-	1.883
O15	-	-	-	-	-	0.107	-	0.932	0.960	-	-	-	-	-	-	1.999
O16	-	-	0.321	-	0.363	-	-	-	-	-	-	-	-	1.102	-	1.786
O17	-	-	-	-	-	-	-	-	-	1.036		0.971	-	-	-	2.006
O18	-	-	-	-	-	0.112	0.934	-	0.993	-	-	-	-	-	-	2.039
O19	-	-	-	-	-	-	-	-	-	1.065	-	-	1.052	-	-	2.116
O20	0.113	-	-	-	-	-	-	-	-	-	-	-	-	0.960	1.036	2.109
O21	0.078	-	-	-	-	-	-	-	-	1.036	0.964	-	-	-	-	2.078
O22	0.151	-	-	-	-	-	-	-	-	-	-	-	0.976	0.993	-	2.120
O23	0.183	-	-	-	-	-	-	-	0.962	-	0.940	-	-	-	-	2.085
Σ	0.978	1.855	1.693	1.732	1.800	0.944	4.055	4.030	4.018	4.126	3.974	4.055	4.030	4.018	4.126	45.725

Valence parameters from [25].

Table 7. Powder X-ray diffraction data for patynite.

d_{obs}	I_{obs}	d_{calc}	I_{calc}	hkl
13.141	12	13.077	86	0 0 1
10.175	8	10.176	5	**0 1 0**
9.364	7	9.300	7	**0 1 −1**
7.030	11	7.171	2	**0 1 1**
6.332	7	6.304	18	**0 1 −2**
5.636	10	5.664	10	**1 −1 −1**
4.947	13	4.943	24	0 1 2
4.618	9	4.650	29	**0 2 −2**
4.220	8	4.211	12	**1 1 −3**
3.844	6	3.846	42	**0 2 −3**
3.454	**100**	**3.459**	**35**	**2 −1 −1**
3.262	**66**	**3.270**	**92**	**2 −1 −2**
3.103	**64**	**3.152**	**100**	**0 2 −4**
2.931	16	2.954	22	1 1 3

Table 7. *Cont.*

d_{obs}	I_{obs}	d_{calc}	I_{calc}	*hkl*
2.801	**21**	**2.786**	**37**	**2 0 −4**
2.592	18	2.630	40	0 4 −1
2.392	10	2.398	14	**0 3 −5**
2.161	8	2.158	12	**2 3 1**
2.124	6	2.127	12	**2 0 4**
2.024	8	2.027	25	**2 −3 4**
1.985	8	1.989	14	**2 −4 3**
1.820	**28**	**1.817**	**77**	**4 0 −2**
1.747	3	1.743	5	**0 6 −3**
1.692	4	1.693	4	**3 0 −7**
1.640	3	1.639	6	**2 3 4**
1.590	4	1.601	19	**0 5 −7**
1.553	6	1.558	10	**4 2 −6**
1.496	5	1.496	11	**4 3 0**
1.455	4	1.456	2	**1 5 4**
1.354	5	1.361	8	**4 −5 2**
1.250	2	1.251	8	**0 8 −6**
1.169	3	1.169	5	**6 0 0**
1.134	3	1.134	2	**3 −1 9**

Bold: the five most intense observed reflections.

5. Description of Crystal Structure and Discussion

Patynite is an inosilicate with tubular columns having an internal channel. Its unique structure can be described as being constituted by two types of modules:

(1) One triple chain of tetrahedrally coordinated Si atoms; the chain extends along the direction of the *a* lattice parameter and is built up by three symmetrically independent wollastonite chains with three tetrahedra in the repeat unit; the triple chain encloses eight-membered and five-membered rings of tetrahedra (Figure 9). The neighboring triple chains (i.e., bands) are not isolated and are related by a center of symmetry and connected in such a way that every third tetrahedron in two of the wollastonite-type chains has a common vertex with a tetrahedron of the centrosymmetric band. Thus, the six wollastonite-type chains build up a complex motif of tetrahedra corresponding to a complex column (a silicate tube) running along the *a*-axis (Figure 13). The stoichiometry of the silicate radical is Si_9O_{23}, and $(Si_{18}O_{46})^{20-}$ is the repeat unit. Each column contains a central channel decorated with lateral strips of eight-membered distorted rings. The channel has lateral windows built of eight-membered rings and five-membered rings adjacent along the *a*-axis, and with saddle-distorted six-membering rings perpendicular to the *a*-axis (Figure 14). This kind of channel is unknown neither in other minerals with tubular silicate radicals nor in zeolites. Potassium atoms occur in the centers of the lateral eight-membered windows of the chain (Figure 14). Na atoms occupy a position within the eight-fold rings of the lateral strips attached to the columns.

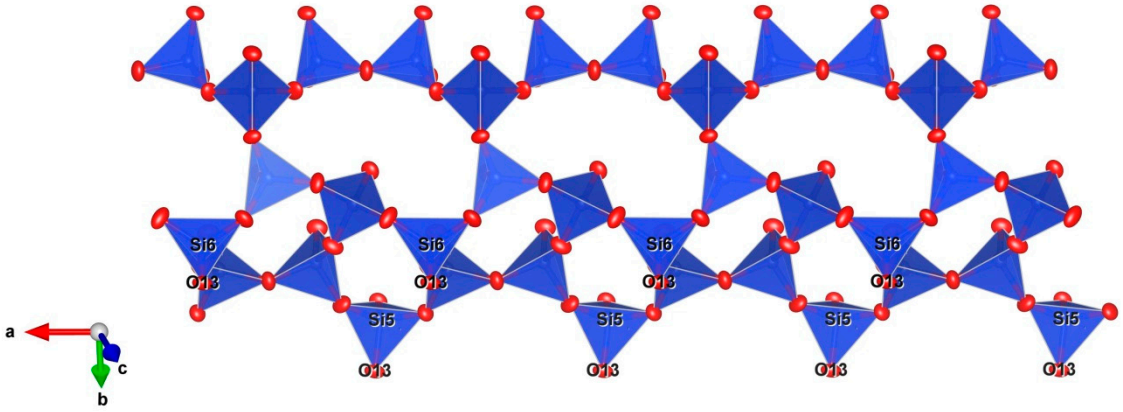

Figure 9. A triple chain in patynite. The periodicity involves every three tetrahedra along the *a*-axis. Two triple chains link by sharing the apex of every third tetrahedron of two of the wollastonite-type single chains, namely via oxygen at the O13 site bridging two silicon atoms at the Si5 and Si6 sites (with the angle Si5–O13–Si6 of 133.5(1)°). The six wollastonite-type single chains configure a complex columnar (tubular) unit with a central channel and lateral rings (see Figures 10–14), with the stoichiometry $[Si_{18}O_{46}]^{20-}$.

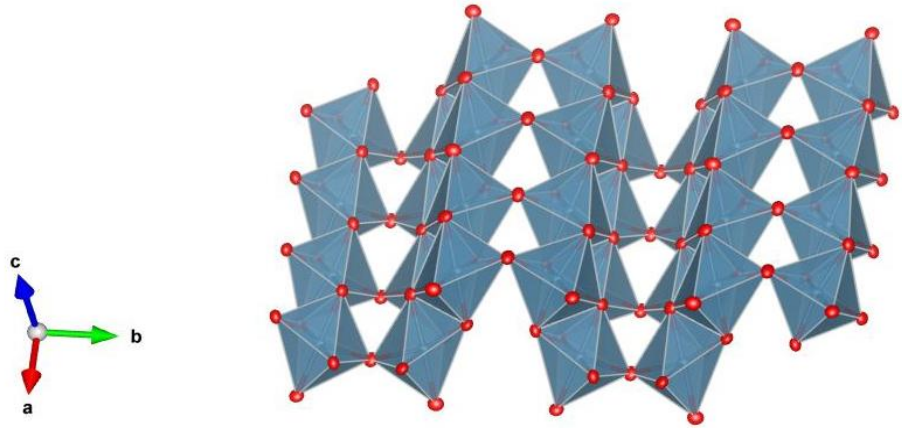

Figure 10. The corrugated layer of the Ca-centered octahedra.

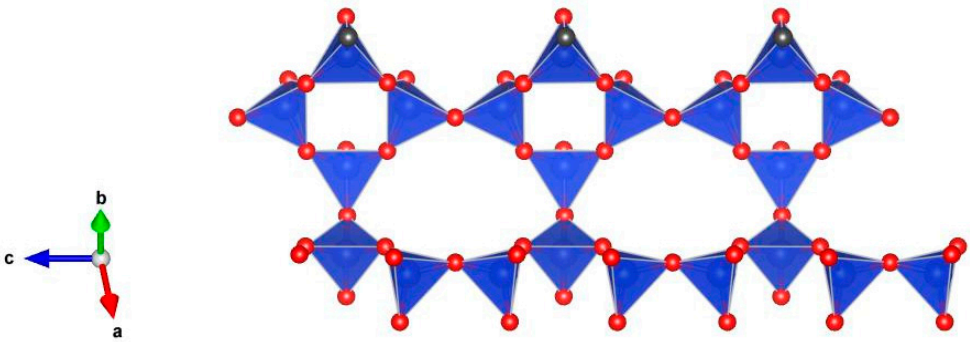

Figure 11. The silicate chain in tokkoite.

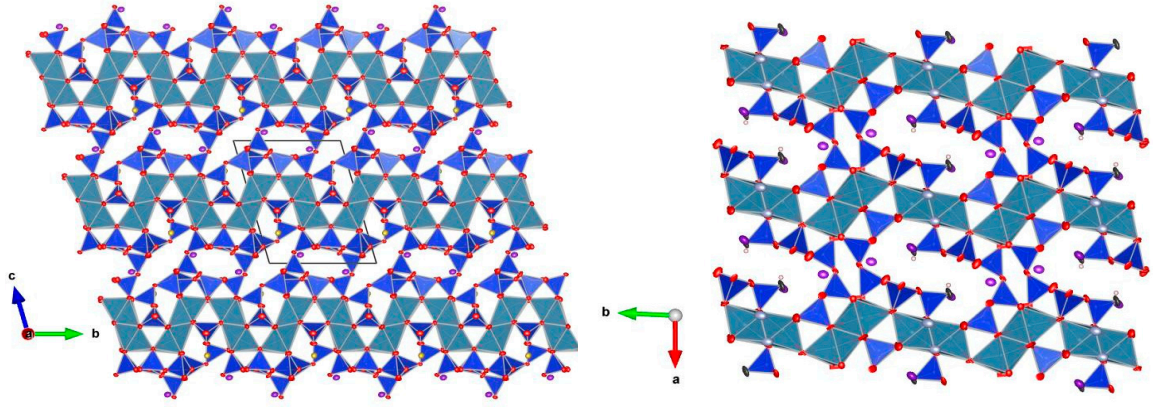

Figure 12. Comparison of "layers" in patynite (**left**) and tokkoite (**right**). K atoms are shown with violet ellipsoids.

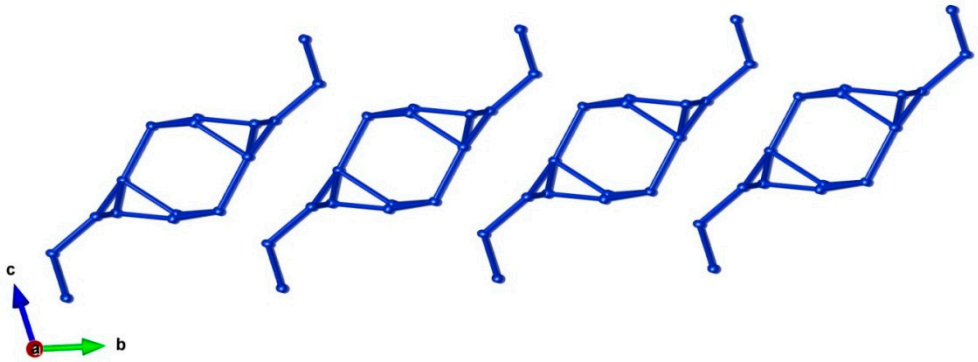

Figure 13. Four consecutive silicate "columns" along the *b*-axis, showing silica polymerization within the $[Si_{18}O_{46}]^{20-}$ units. Only the Si sites and Si–Si distances are represented to evidence the branched tubular topology of the complex silicate unit. Two centrosymmetric triple chains (Figure 5) link by sharing the oxygen apex of every two Si tetrahedra, resulting in the decorated column or silicate tube with a channel.

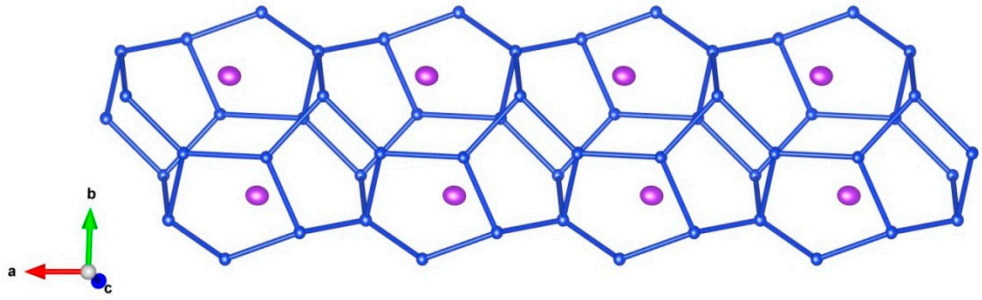

Figure 14. Detail of the backbone of the central silicate "channel" (tube) in the $[Si_{18}O_{46}]^{20-}$ units of patynite. Only the Si sites and Si–Si distances are represented to evidence the topology of the complex silicate unit. Two centrosymmetric triple chains (Figure 9) link by sharing the oxygen apex of every third Si tetrahedron of four chains configuring a sort of decorated column (silicate tube) with a channel. The external chains are not represented for simplicity. The sites at the centers of the lateral eight-membered rings host K cations (violet ellipsoids) whereas the central part of the channel is empty.

(2) Ca-centered octahedra sharing common edges form a two-fold strip running along the *a* lattice parameter. Adjacent strips link along the *b* lattice parameter by sharing common apexes to form a corrugated octahedral layer extending on the (001) plane (Figure 10).

The other minerals whose crystal structures contain tubular silicate radicals are charoite, agrellite, and miserite [26], as well as members of the litidionite group, which includes litidionite, fenaksite,

manaksite, and calcinaksite [27]. All these minerals differ significantly from patynite in the structures of the silicate tubes, chemical composition, and IR spectra.

The silicate radical of patynite is different from those of tokkoite and tinaksite [8,9] which have the stoichiometry $[Si_7O_{18}(OH)]^{9-}$ and are built up by unbranched double chains of Si tetrahedra, which form eight- and four-membered rings (Figure 11). The corrugated layers of Ca-octahedra in tokkoite and tinaksite is also topologically different (Figure 12).

Based on the structural data described above, patynite can be considered as a prototype of a material with heteropolyhedral structure that is capable of the selective accumulation and immobilization of large cations in structural channels.

Supplementary Materials: The CIF file (containing all crystallographic information) and the hkl file (containing all hkl reflections) are available online at http://www.mdpi.com/2075-163X/9/10/611/s1.

Author Contributions: V.S.L. collected the material in situ, A.V.K. found the new mineral; F.C. and F.N. performed the X-ray structural investigations; R.Š. and A.V.K. conducted the electron-microprobe analyses and obtained Raman spectrum; N.V.C. obtained IR spectrum and analyzed IR and Raman data; A.A.A. and D.I.B. determined the physical, chemical, and optical properties; A.V.K., F.C., N.V.C., and F.N. wrote the paper.

Funding: A part of this work (infrared spectroscopy and, partly, crystal-chemicalanalysis) was financially supported by the Russian Foundation for BasicResearch, grant no. 18-29-12007-mk.

Acknowledgments: The reviewers and guest editor are acknowledged for their constructive comments.

Conflicts of Interest: The authors declare no conflict of interest.

References

1. Chukanov, N.V.; Aksenov, S.M.; Rastsvetaeva, R.K.; Blass, G.; Varlamov, D.A.; Pekov, I.V.; Belakovskiy, D.I.; Gurzhiy, V.V. Calcinaksite, $KNaCa(Si_4O_{10})\cdot H_2O$, a new mineral from the Eifel volcanic area, Germany. *Mineral. Petrol.* **2015**, *109*, 397–404. [CrossRef]
2. Dorfman, M.D.; Rogachev, D.D.; Goroshchenko, Z.I.; Uspenskaya, E.I. Canasite, a new mineral. *Trudy Mineral. Muzeya Akad. Nauk SSSR* **1959**, *9*, 158–166. (In Russian)
3. Rozhdestvenskaya, I.V.; Nikishova, L.V.; Bannova, I.I.; Lasebnik, Y.D. Canasite: The refinement of crystal structure and comparison with that of miserite. *Acta Crystallogr.* **1987**, *43*, C159. [CrossRef]
4. Khomyakov, A.P.; Nechelyustov, G.N.; Krivokoneva, G.K.; Rastsvetaeva, R.K.; Rozenberg, K.A.; Rozhdestvenskaya, I.V. Fluorcanasite, $K_3Na_3Ca_5Si_{12}O_{30}(F,OH)_4\cdot H_2O$, a new mineral from Khibiny Alkaline Massif (Kola Peninsula, Russia) and new data on canasite. *Zap. Ross. Mineral. Obsh.* **2009**, *138*, 52–66. (In Russian)
5. Nikishova, L.V.; Lazebnik, K.A.; Rozhdestvenskaya, I.V.; Emelyanova, N.N.; Lazebnik, Y.D. Frankamenite $K_3Na_3Ca_5(Si_{12}O_{30})F_3(OH)\cdot H_2O$—A new mineral, triclinic variety of canasite from charoitites. *Zap. Vser. Mineral. Obsh.* **1996**, *125*, 106–108. (In Russian)
6. Rozhdestvenskaya, I.V.; Nikishova, L.V.; Lazebnik, K.A. The crystal structure of frankamenite. *Mineral. Mag.* **1996**, *60*, 897–905. [CrossRef]
7. Rogov, Y.G.; Rogova, V.P.; Voronkov, A.A.; Moleva, V.A. Tinaksite $NaK_2Ca_2TiSi_7O_{19}(OH)$, a new mineral. *Dokl. Akad. Nauk SSSR* **1965**, *162*, 658–661. (In Russian)
8. Rozhdestvenskaya, I.V.; Nikishova, L.V.; Lazebnik, Y.D.; Lazebnik, K.A. The crystal structure of tokkoite and its relation to the structure of tinaksite. *Z. Kristallogr.* **1989**, *189*, 195–204.
9. Lacalamita, M.; Mesto, E.; Kaneva, E.; Scordari, F.; Pedrazzi, G.; Vladykin, N.; Schingaro, E. Structure refinement and crystal chemistry of tokkoite and tinaksite from the Murun massif (Russia). *Mineral. Mag.* **2017**, *81*, 251–272. [CrossRef]
10. Ilyenok, S.S. Osnovnye cherty petrologii Patynskogo massiva (Main features of the Petrology of Patynskiy massif). *Geologiya I geofizika (Geol. Geophys.) SO AN SSSR* **1960**, *4*, 76–91. (In Russian)
11. Ilyenok, S.S. *Petrologiya gabbro-siyenitovogo complexa Gornoy Shorii (Petrology of Gabbro-Syenite Complex of Gornaya Shoriya)*; Tomsk University: Tomsk, Russia, 1964; p. 130. (In Russian)
12. Dovgal, V.N. *Rannepaleozoyskaya gabbro-siyenitovaya formatsiya tsentralnoy tchasti Altae-Sayanskoy skladtchatoy oblasti (Early Paleozoic Gabbro Syenite Formation of the Central Part of Altai-Sayany Folded Area)*; Nauka: Moscow, Russia, 1968; p. 207. (In Russian)

13. Belyaev, E.V. The Polygenous Nature of the Patyn Ore-Magmatic Cluster (Mountainous Shoriya). *Dokl. Earth Sci.* **2010**, *435*, 1420–1422. [CrossRef]
14. Rogova, V.P.; Rogov, Y.G.; Drits, V.A.; Kuznetsova, N.N. Charoite, a new mineral, and a new jewelry stone. *Zap. Vses. Mineral. Obsh.* **1978**, *107*, 94–100. [CrossRef]
15. Nikishova, L.V.; Lazebnik, K.A.; Lazebnik, Y.D. About the crystallochemical formula of charoite. In *Crystal Chemistry and Structure of Minerals*; Nauka: Leningrad, Russia, 1985; pp. 100–105.
16. Rozhdestvenskaya, I.; Mugnaioli, E.; Czank, M.; Depmeier, W.; Kolb, U.; Reinholdt, A.; Weirich, T. The structure of charoite, $(K,Sr,Ba,Mn)_{15\text{-}16}(Ca,Na)_{32}[(Si_{70}(O,OH)_{180})](OH,F)_{4.0}{\cdot}nH_2O$, solved by conventional and automated electron diffraction. *Mineral. Mag.* **2010**, *74*, 159–177. [CrossRef]
17. Lazebnik, K.A.; Nikishova, L.V.; Lazebnik, Y.D. Tokkoite—A new mineral of charoitites. *Mineralog. Zhurnal* **1986**, *8*, 85–89. (In Russian)
18. Mandarino, J.A. The Gladstone-Dale relationship. IV. The compatibility concept and its 209 application. *Can. Mineral.* **1981**, *41*, 989–1002.
19. Sitarz, M.; Mozgawa, W.; Handke, M. Vibrational spectra of complex ring silicate anions—Method of recognition. *J. Mol. Struct.* **1997**, *404*, 193–197. [CrossRef]
20. Chukanov, N.V. *Infrared Spectra of Mineral Species: Extended Library*; Springer: Dordrecht, The Netherlands; Heidelberg, Germany; New York, NY, USA; London, UK, 2014; p. 1716.
21. Sheldrick, G.M. A short history of SHELX. *Acta Crystallogr.* **2008**, *A64*, 112–122. [CrossRef] [PubMed]
22. Farrugia, L.J. WinGX and ORTEP for Windows: An update. *J. Appl. Crystallogr.* **2012**, *45*, 849–854. [CrossRef]
23. Holland, T.J.B.; Redfern, S.A.T. Unit cell refinement from powder diffraction data: The use of regression diagnostics. *Mineral. Mag.* **1995**, *61*, 65–77. [CrossRef]
24. Westrip, S.P. publCIF: Software for editing, validating and formatting crystallographic information files. *J. Appl. Crystallogr.* **2010**, *43*, 920–925. [CrossRef]
25. Gagné, O.C.; Hawthorne, F.C. Comprehensive derivation of bond-valence parameters for ion pairs involving oxygen. *Acta Crystallogr.* **2015**, *B71*, 562–578. [CrossRef] [PubMed]
26. Rozhdestvenskaya, I.V.; Krivovichev, S.V. Tubular chains in the structures of natural and synthetic silicates. *Crystallogr. Rep.* **2011**, *56*, 1007–1018. [CrossRef]
27. Aksenov, S.M.; Rastsvetaeva, R.K.; Chukanov, N.V.; Kolitsch, U. Structure of calcinaksite $KNa[Ca(H_2O)][Si_4O_{10}]$, the first hydrous member of the litidionite group of silicates with $[Si_8O_{20}]^{8-}$ tubes. *Acta Crystallogr. B* **2014**, *70*, 768–775. [CrossRef] [PubMed]